Available online at www.sciencedirect.com
ScienceDirect
Planetary and Space Science 54 (2006) 1498–1509
Planetary and Space Science
www.elsevier.com/locate/pss

Titan: Preliminary results on surface properties and photometry from VIMS observations of the early flybys

B.J. Buratti[a,*], C. Sotin[b], R.H. Brown[c], M.D. Hicks[a], R.N. Clark[d], J.A. Mosher[a], T.B. McCord[e], R. Jaumann[f], K.H. Baines[a], P.D. Nicholson[g], T. Momary[a], D.P. Simonelli[a], B. Sicardy[h]

[a]*Jet Propulsion Laboratory, Mail stop 183-501, Pasadena, CA 91109, USA*
[b]*University of Nantes, B.P. 92208, 2 rue de la Houssinière, 44072 Nantes Cedex 3, France*
[c]*Department of Planetary Science and LPL, University of Arizona, Tucson, AZ 85721-0092, USA*
[d]*USGS, Mail Stop 964, Box 25046, Denver Federal Center, Denver, CO, USA*
[e]*Space Science Institute, 22 Fiddler's Rd., Winthrop, WA 98862-0667, USA*
[f]*DLR, Institute for Planet. Expl., Rutherfordstrasse 2, D-12489 Berlin, Germany*
[g]*Department of Astronomy, Cornell University, Ithaca, NY 14853, USA*
[h]*Observatoire de Paris, 5 Place Jules Janssen, F-92195 Meudon Cedex, France*

Accepted 9 June 2006
Available online 30 August 2006

Abstract

Cassini observations of the surface of Titan offer unprecedented views of its surface through atmospheric windows in the 1–5 μm region. Images obtained in windows for which the haze opacity is low can be used to derive quantitative photometric parameters such as albedo and albedo distribution, and physical properties such as roughness and particle characteristics. Images from the early Titan flybys, particularly T0, Ta, and T5 have been analyzed to create albedo maps in the 2.01 and 2.73 μm windows. We find the average normal reflectance at these two wavelengths to be 0.15 ± 0.02 and 0.035 ± 0.003, respectively. Titan's surface is bifurcated into two albedo regimes, particularly at 2.01 μm. Analysis of these two regimes to understand the physical character of the surface was accomplished with a macroscopic roughness model. We find that the two types of surface have substantially different roughness, with the low-albedo surface exhibiting mean slope angles of ~18°, and the high-albedo terrain having a much more substantial roughness with a mean slope angle of ~34°. A single-scattering phase function approximated by a one-term Henyey–Greenstein equation was also fit to each unit. Titan's surface is back-scattering (g~0.3–0.4), and does not exhibit substantially different backscattering behavior between the two terrains. Our results suggest that two distinct geophysical domains exist on Titan: a bright region cut by deep drainage channels and a relatively smooth surface. The two terrains are covered by a film or a coating of particles perhaps precipitated from the satellite's haze layer and transported by eolian processes. Our results are preliminary: more accurate values for the surface albedo and physical parameters will be derived as more data is gathered by the Cassini spacecraft and as a more complete radiative transfer model is developed from both Cassini orbiter and Huygens Lander measurements.

Keywords: Titan; Saturnian satellites; Cassini mission

1. Introduction and scope

Titan is the most interesting planetary satellite, exhibiting features and phenomena that place it in kinship to the Earth. With a thick atmosphere composed mainly of nitrogen, massive volcanic features with associated flows (Elachi et al., 2005) smaller cryovolcanoes (Sotin et al., 2005), dendritic features suggestive of surface fluid flow, possible lakes, eolian features, enigmatic "cat scratches", and apparently low crater counts on most parts of the surface, this satellite has spawned intense scientific interest and controversy. The few percent methane and optically thick aerosols in its atmosphere have obscured the surface

*Corresponding author. Tel.: +1 818 354 7427 fax: +1 818 354 0966.
E-mail address: bonnie.buratti@jpl.nasa.gov (B.J. Buratti).

0032-0633/$ - see front matter © 2006 Elsevier Ltd. All rights reserved.
doi:10.1016/j.pss.2006.06.015

from terrestrial visual observers, but the relatively narrow windows in the near IR have been exploited to construct rotational lightcurves and rough surface maps (Lemmon et al., 1993, 1995; Lellouch et al., 2004). These lightcurves revealed a global leading-trailing albedo asymmetry, and a high-albedo region dubbed Xanadu observed with HST and Keck dominates the longitudinal range 60°–150° (Smith et al., 1996; Roe et al., 2004; Gibbard et al., 2004; Coustenis et al., 2005). Adding to the mystery of Titan are strongly peaked radar signals that suggested the presence of liquids, or at least a very flat surface (Campbell et al., 2003). On the other hand, ground-based IR observations that show the absence of a specular "glint" that would appear if liquid were present seem to preclude the existence of large areas of liquid on the surface (West et al., 2005).

The Cassini visual infrared mapping spectrometer (VIMS) is an imaging system that has 352 channels over the spectral range of 0.35–5.2 μm and a spatial resolution of up to 0.25 mrad (0.17 mrad in the visual). It is ideally suited for studying the surface properties of Titan, particularly in the infrared bands where the methane opacity drops dramatically (Fig. 1). The details of the VIMS instrument are described in Brown et al., 2004. In this paper we examine VIMS observations from the early Cassini flybys of Titan, primarily T0, Ta, and T5, to make preliminary determinations of the surface properties of the satellite, including the surface geometric albedo and its distribution; global composition; the surface phase function; and physical properties including macroscopic roughness and the single-particle-phase function. Because haze opacity is substantial even in the methane windows, ranging from a normal optical depth of unity at 1.0 μm, to 0.10 at 2.0 μm, and less at 5.0 μm (Griffith et al., 2003), we perform a simple haze correction to our observations. Our results are first look: the gathering of data during 39 close flybys in the remaining 3 years of the nominal mission and the development of a full radiative transfer model to separate the contribution of the atmosphere and haze from that of the surface will happen during the coming years.

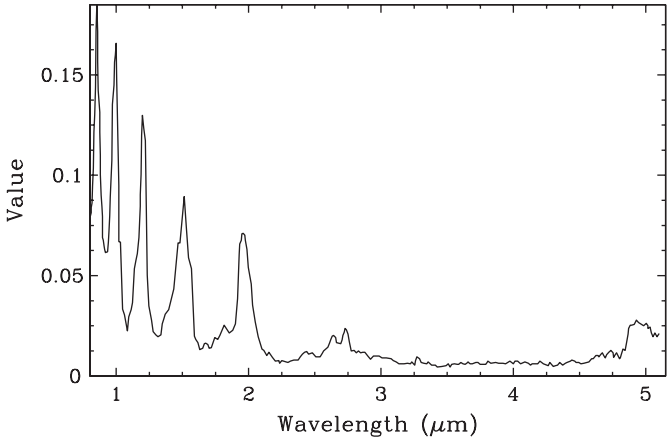

Fig. 1. A typical spectrum of Titan, showing the atmospheric windows at 0.93, 1.07, 1.28, 1.57, 2.01, 2.73, and 4.94 μm.

Our study is meant to understand the basic morphology of Titan's surface and to compare these results with the surfaces of other satellites and planets.

2. Description of data

Prior to Saturn orbit insertion (SOI), during SOI, and during the first year of the 4-year nominal Cassini Mission (July 1, 2004–July 1, 2005) several important sets of Titan data were returned. During the last weeks of cruise, thousands of unresolved observations of Titan were obtained: these were designed to obtain a complete rotational lightcurve of the body, and to gather the first spectra of it. Within hours after SOI the spacecraft turned to Titan to take advantage of a "first glimpse" during a serendipitous close approach of about 340,000 km. This untargeted flyby was called T0, as it occurred before any of the targeted flybys. The first targeted close flyby (Ta) occurred on October 26, 2004, followed by flybys in December 14, 2004 (Tb), February 15, 2005 (T3), March 31, 2005 (T4), and April 16, 2005 (T5). The observations used in this analysis are listed in Table 1. We focused primarily on Ta and T5 because they have complementary surface coverage (see Fig. 2). The observations from T0 were included to increase the excursion in solar phase angle for our derivation of Titan's solar phase function (the solar phase angle changes by only 1–2° for the main data obtained in Ta and T5). Because the spacecraft trajectory causes the same photometric and geographical geometries to be repeated during flybys, a complete range in phase angles and surface coverage at high spatial resolution will take the entire 4-year tour (and even then, much coverage will be missing, particularly at the highest spatial resolution).

3. Data analysis

All observations were calibrated to absolute radiance measurements of specific intensity reference to the incident solar flux (I/F) using extensive preflight calibrations described in Brown et al. (2004) augmented by inflight observations of stars and targets in the Saturnian system. Pointing geometry, including solar phase, incidence, and emission angles, subobserver latitude and longitude, and spacecraft range were provided by the Navigation Team (see Table 1 for average values of these parameters; for disk-resolved images they were calculated for each pixel).

3.1. Rotational lightcurves

Titan's rotational lightcurve was constructed from the nearly 3000 images that were obtained during cruise prior to SOI. The disk-integrated observations were created by summing the flux in every pixel that included a signal from Titan and correcting to a common spacecraft distance. The resulting data were coadded into 5° bins in subspacecraft longitude; additional coadding was done for the 4.94 μm

Table 1
Summary of observations used in this study

Titan flyby	Observation title	Date	Time (UT)	Exp (ms)	Spatial mode	Array size (ns–nl)	Number of cubes	Subobserver		Phase angle (deg)	Range (10^5 km)	Spatial resolution (km pix^{-1})
								Longitude (deg)	Latitude (deg)			
Cruise	LIGHTC	2004-May-23 to June-11		320 80	Normal	12–12	2820	Full range	15–18	64–72	130-220	Titan sub-pixel
T0	SPOLEA	2004-July-03	01:56	320 80	Hi-res	42 × 30	20	350	−35	48–64	3.43–4.08	86–102
T0	SPOLEB	2004-July-03	09:30	240,100,200	Hi-res	42 × 36	6	Range	−60	67–69	3.42	86
TA	MEDRES001	2004-Oct-26	04:12	40	Normal	54–54	1	160	−15	13	2.33	116
TA	MEDRES001	2004-Oct-26	04:16	80	Normal	54–54	1	160	−15	13	2.32	116
TA	MEDRES001	2004-Oct-26	04:22	160	Normal	54–54	1	160	−15	13	2.29	115
TA	MEDRES001	2004-Oct-26	04:33	320	Normal	54–54	1	160	−15	13	2.25	112
TA	MEDRES001	2004-Oct-26	04:53	640	Normal	64–64	1	161	−15	13	2.18	109
TA	MEDRES001	2004-Oct-26	05:41	1200	Normal	64–64	1	161	−15	13	2.02	101
TA	MEDRES001	2004-Oct-26	07:11	320	HI-res	64–64	1	162	−14	13	1.71	42.8
TA	MEDRES001	2004-Oct-26	07:35	640	Hi-res	64–64	1	163	−14	13	1.63	40.7
TA	MEDRES001	2004-Oct-26	08:28	120	Hi-RES	64–64	1	163	−14	13	1.44	36.1
TA	MEDRES001	2004-Oct-26	08:45-10:05	160	Hi-res	64–64	6	164	−14	13	1.22	30.5
T5	MEDRESMAP	2005-Mar-31	11:37	320	Hi-res	24–12	1	1	−18	57	1.73	43.3
T5	MEDRESMAP	2005-Mar-31	11:46-14:17	80	Hi-res	24–12	23	1	−20	57	1.39	34.8
T5	MEDRESMAP	2005-Mar-31	11:49-14:14	480	Hi-res	24–12	23	1	−20	57	1.39	34.8

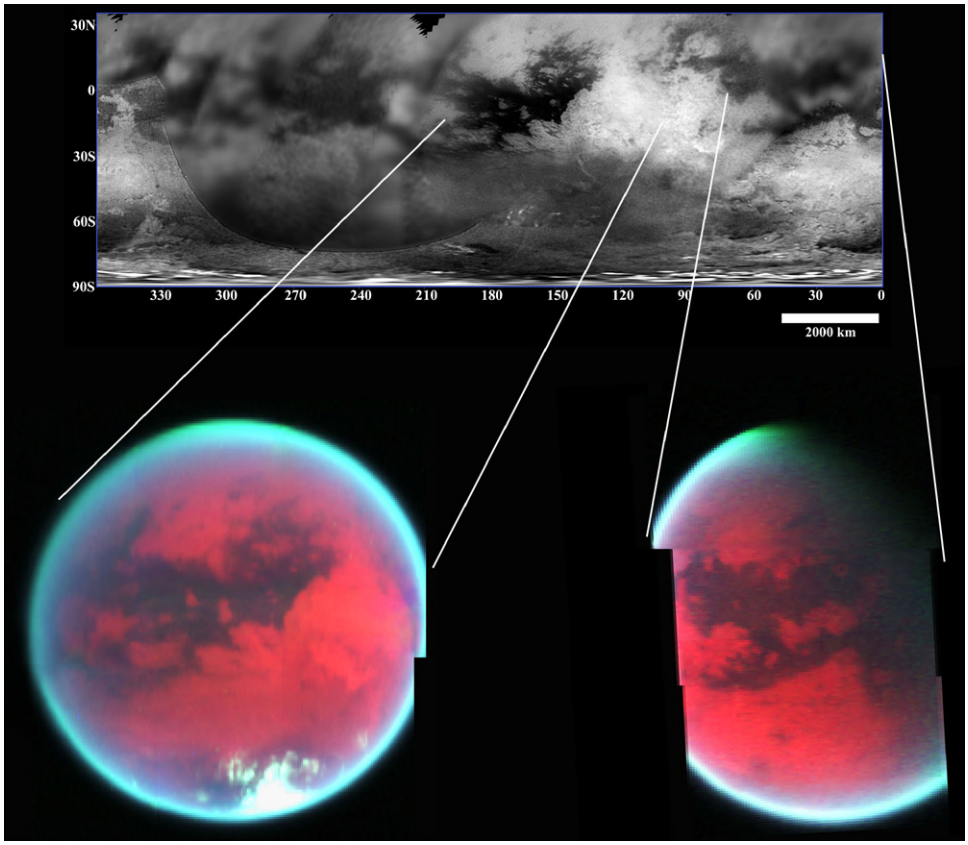

Fig. 2. Color composite maps of Ta and T5 shown with the Imaging Science Subsystem mosaic, obtained at http://cassini.jpl.nasa.gov. The wavelengths used in this rendition are 2.0, 2.83, and 2.13 μm for the red, green, and blue channels.

data to improve the signal-to-noise. In addition, the 4.94 μm lightcurve consists of the coaddition and average of all the wavelengths from 4.87–5.01 μm. The resulting rotational lightcurves for the main atmospheric windows are shown in Fig. 3, along with previous ground-based results (the data are shown with longitude increasing to the East, to conform to IAU convention with which the ground-based data were published). In the wavelengths where ground based information exists—the windows at 1.07, 1.28, 1.57, 2.01, and 4.94 μm—there is good agreement with the VIMS data, providing validation of the instrument's status and radiometric fidelity. These results confirm the existence of a hemispheric dichotomy on the satellite, and when they are combined with the ground-based near-IR maps, it becomes clear that the high-albedo region from 0°–150° (Xanadu) causes the maximum in the lightcurve, while the minimum on the opposite hemisphere is due to the preferential placement of low-albedo terrain there. At wavelengths where the VIMS lightcurve is new, in the atmospheric window at 0.93 and at 4.26 μm (the later wavelength chosen as representative of the 3–4.85 μm region), and at the important atmospheric windows at 2.73 and 4.94 μm, the hemispheric dichotomy is also obvious. Fig. 4 shows the lightcurve amplitude and the haze opacity (Griffith et al., 2003) as a function of wavelength: in the windows where the opacity is lowest (2.01 and 4.94 μm) the lightcurve amplitude is greatest. This result suggests the lightcurve amplitude is tracking surface features, and it provides a key to the wavelengths that are best for studying the morphologic and photometric properties of Titan's surface: 2.01, 2.73 and 4.94 μm.

3.2. Albedo maps and histograms

Lightcurves yield information on the global distribution of bright and dark material on a planetary surface, but albedo maps enable detailed investigations of questions such as: is albedo correlated with geologic features? Is the albedo grouped into distinct ranges? Does the albedo distribution change with wavelength? To construct a map that shows intrinsic albedo, or a map of normal reflectance, two important corrections for viewing geometry must be carefully modeled: the changes in intensity due to changing incidence and emission angle ("limb darkening"), and changes due to the solar phase angle alone. To correct for limb darkening, the following equation was used:

$$I(\mu, \mu_0, \alpha)/F = f(\alpha) r_n \mu_0 / \pi(\mu + \mu_0), \quad (1)$$

where I is the specific intensity, πF is the incidence solar flux, r_n is the normal reflectance, μ and μ_0 are the cosines of the emission and incidence angles, respectively, and $f(\alpha)$ is a function that depends only on the effects of solar phase.

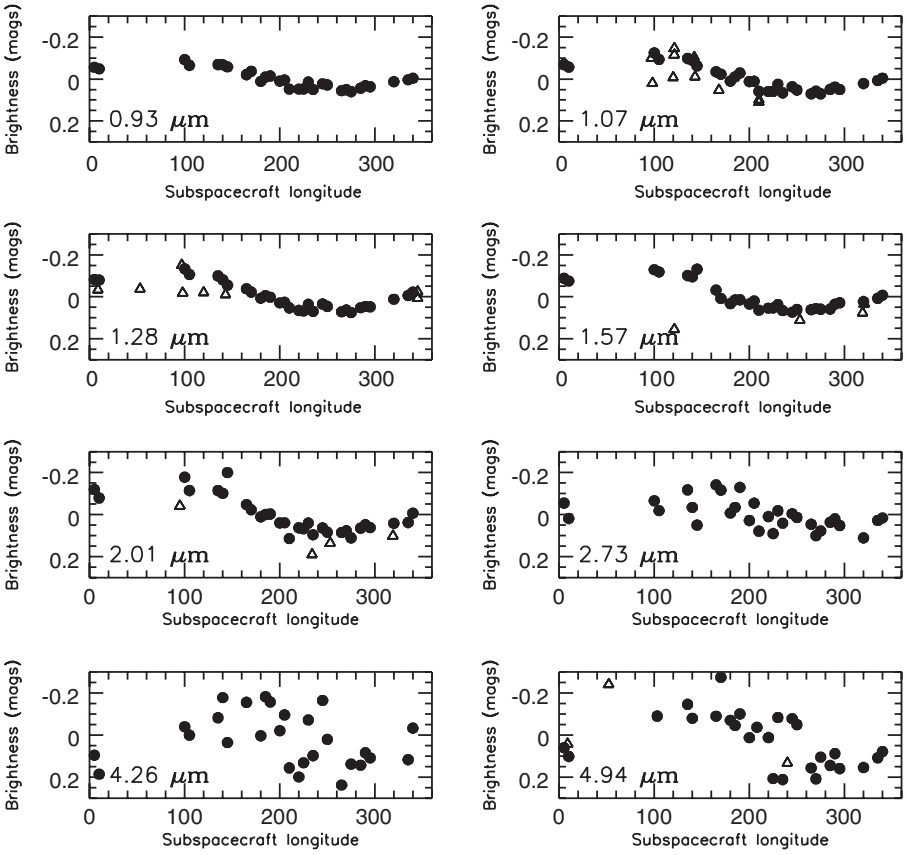

Fig. 3. Rotational lightcurves of Titan shown in 8 atmospheric windows. The filled circles are the Cassini VIMS observations, while the open triangles are ground-based observations from Lemmon et al. (1995) and Lellouch et al. (2004).

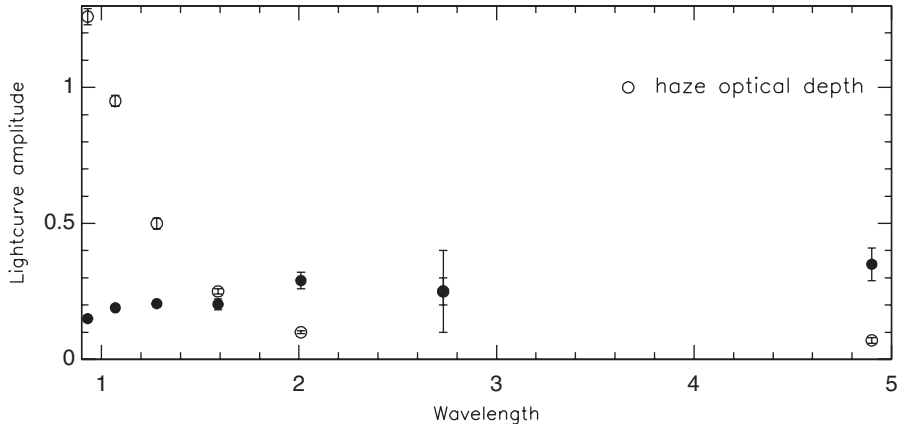

Fig. 4. Opacity of Titan's atmosphere (Griffith et al., 2003) vs. lightcurve amplitude, which are shown as black dots. The lightcurve amplitude is highest where the opacity is lowest, which confirms that the variations in the lightcurve are due to surface features.

This equation is known as a lunar or Lommel–Seeliger scattering law, and is a good approximation for icy satellites that have geometric albedos less than 0.6 (Buratti, 1984). The function $f(\alpha)$ contains important physical information about the surface, which will be derived later in this section. For this preliminary study, two wavelengths where atmospheric transmission is at a maximum were used to derive surface albedo: 2.01 and 2.73 μm (the 5 μm region also has low atmospheric opacity and even lower haze opacity, but the VIMS signal to noise in this spectral region is much worse, so that region was not studied). Before corrections for viewing geometry were done, a haze correction using the values given in Griffith et al. (2003) were done (the value for 2.73 μm, which was not examined by Griffith et al., was interpolated from their values, under the assumption that the haze opacity varies slowly with

wavelength). The specific numbers we used for atmospheric extinction were 10% per unit airmass for 2.01 μm and 25% per unit airmass for 2.73 μm. These corrections are preliminary, and more accurate numbers will be derived as more complete radiative transfer models are derived from both Cassini orbiter and Huygens lander analyses. Correction factors to 0° phase angle were 1.04 for Ta and 1.17 for T5 for both wavelengths; this correction was based on a phase coefficient of 0.003 mag/deg derived from the measured integral brightness of Titan as a function of solar phase angle, corrected for the rotational light curve. The phase angle changes by one degree or less over the images used; thus the same phase correction can be used for the entire image. The results are shown in Fig. 5.

The average normal reflectance of Titan at 2.01 μm is 0.15 ± 0.02, and at 2.73 μm it is 0.035 ± 0.003. The histograms at both wavelengths show a wide range in surface albedo, but there is a clear bifurcation, indicating that there are two distinct albedo terrains on the satellite. The average normal reflectances for these two terrains are

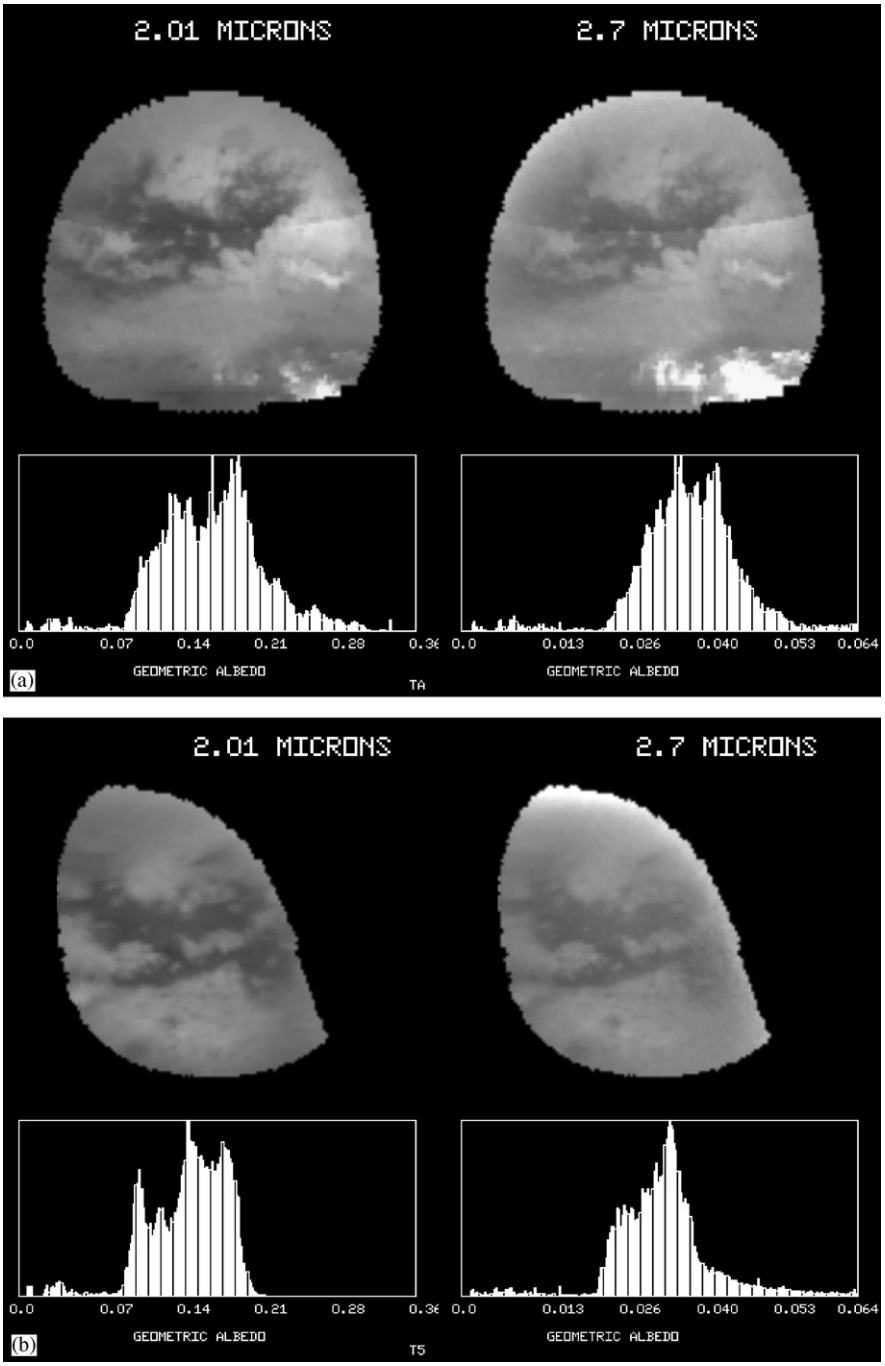

Fig. 5. (a) and (b) Maps of geometric albedo (normal reflectance) produced from global mosaics constructed from the Ta and T5 flybys. The maps have been corrected for limb darkening, haze, and solar-phase effects.

about 0.12 and 0.17 at 2.01 μm and about 0.033 and 0.038 at 2.73 μm, corresponding to an albedo variation of about 40% at 2.01 μm and about 15% at 2.73 μm. Our value at 2 μm is in fair agreement with the Griffith et al. (2003) value of 0.12 ± 0.01, while Gibbard et al. (2004) published an albedo map of Titan at 2.1 μm from Keck Telescope speckle and adaptive optics with substantially lower numbers, ranging from 0.02 to 0.10. Coustenis et al. (2005) present maps at 2 μm based on three adaptive optics systems that show normalized albedo ranges of a factor of 2–2.5, in good agreement with our own ranges.

The final maps of normal reflectance help us address the use of our ad hoc haze correction model. Our model does not account for any changes that may have taken place in Titan's haze opacity in the last 4 years, and the scattering of sunlight by the haze itself has also not been accounted for. If errors due to these two factors were large, they would show up as limb brightening in our final albedo maps and no such effect occurs. For example, compare the haze that appears prominently at Titan's limb in Fig. 2, and the lack of any such haze in our corrected albedo maps. Nevertheless, these maps are to be regarded as preliminary works as additional information on Titan's atmosphere and haze properties are deduced and incorporated into a full radiative transfer model.

3.3. Physical properties of the surface

The visibility of Titan's surface through the infrared atmospheric windows enables for the first time its physical characterization with the photometric techniques that have been widely used for airless bodies' surfaces, including satellite surfaces (e.g., Buratti, 1985; Helfenstein et al., 1988; Domingue et al., 1991; Verbiscer and Veverka, 1992). The moderate and large phase angles covered so far during the mission are especially suited to deriving the roughness and single-particle-phase function of the surface (Helfenstein et al., 1988). As the spacecraft trajectory enables the collection of additional phase angles and geographic areas during the next 2 years, more complete analyses will be accomplished; our current results are to be considered only preliminary.

Macroscopic roughness encompasses facets ranging in size from aggregates of particles to mountains, craters and ridges. These features alter the specific intensity of a planetary surface in two ways: the local incidence and emission angles are changed by alteration of the surface profile from that of a smooth sphere; and they remove radiation from the scene by casting shadows. Two formalisms have been developed to quantitatively model this effect: the Hapke (1984) mean slope model, and the crater roughness model (Buratti and Veverka, 1985). We make use of the crater roughness model, which has been applied to 19P/Borrelly (Buratti et al., 2004), and to Phoebe (Simonelli et al., 2004). The disk-resolved form of the model is particularly useful because it relates surface roughness to limb darkening, which occurs as the emission angle changes, rather than to solar-phase angle. Another problem with using an extensive excursion in solar-phase angle to derive roughness is that roughness is convolved with other effects (such as the single-particle-phase function) and thus it cannot be derived uniquely.

Although roughness models are useful for seeking comparative differences in surface roughness among planetary surfaces and among different terrains on the same body, they have important limitations. The first is that they are scale-invariant: the model includes rough features of all sizes, from clumps of particles to mountains and craters. An analysis by Shepard and Campbell (1998) shows that sizes at the small end tend to dominate. However, this limitation can also be interpreted as a powerful aspect of the model, as it enables the detection of roughness below the resolution limit of the instrument that gathered the data. Another limitation is that the rough shapes are idealized, whether they are mean slopes or bowl-shaped holes (''craters''). The two most widely used models do show fairly similar effects, particularly in a comparison of limb darkening, which is the main technique we use in this paper (Buratti and Veverka, 1985; Hapke, 1984).

The problem of calculating the photometric effects of macroscopic roughness entails both computing the local incidence and emission angles on a surface covered with rough features, and computing the fraction of illuminated surface that is lost to facets blocking solar radiation. Our model assumes that the surface is covered with nonoverlapping bowl-shaped (paraboloidal) features defined by their depth to radius ratio, $q = h/R$, where h is the central depth of the crater and R is its radius. The model specifies the fraction of the surface covered by the craters, and it describes the specific intensity as a function of the incidence, emission, and phase angles and an arbitrary photometric function. The normal reflectances derived earlier indicate that Titan's surface at mid-infrared wavelengths is well-described by a Lommel–Seeliger (lunar) photometric function described by Eq. (1) (see Buratti, 1984; Veverka et al., 1978). Our model produces three equations that guarantee that each point is (1) inside the crater, (2) visible to the observer, and (3) illuminated. Our computer program then calculates the incidence, emission, and phase angles inside the crater on a 50×50 square grid. The photometric function and the solar-phase function are both specified. The amount of light reflected at each point is then computed and the sum of all such contributions is normalized by the area of the crater.

Fig. 6 shows a family of theoretical curves of the specific intensity (I/F) as a function of the radiance emission angle for various depth-to-diameter ratios for the viewing conditions of Ta. The curves show that the maximum point of the curve is a sensitive indicator of the degree of macroscopic roughness: a smooth surface exhibits no inflection point while as the roughness increases, the maximum point moves to progressively smaller emission angles. This figure illustrates that it is not necessary to obtain large numbers of observations at large solar phase

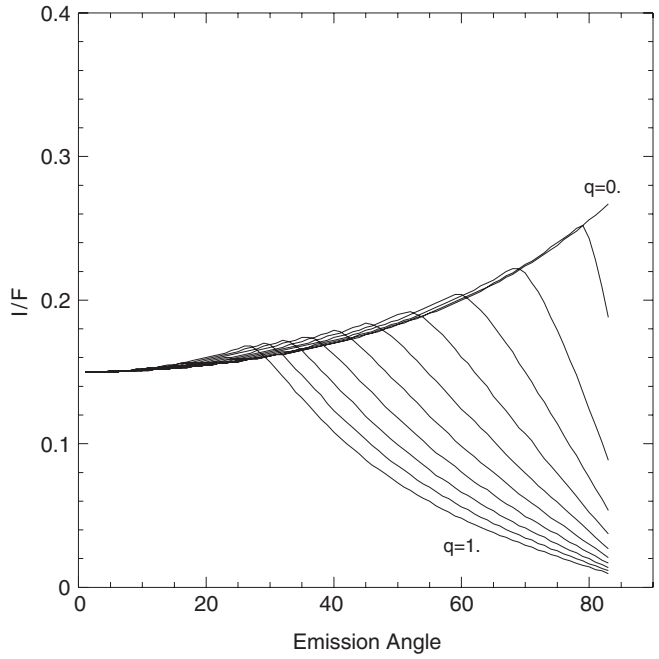

Fig. 6. A family of scans of I/F vs. radiance emission angle for the roughness model, based on the geometry for Ta. The 11 curves represent a depth to radius value (q) ranging from 0 (no rough facets) to 1.0 in 0.1 increments.

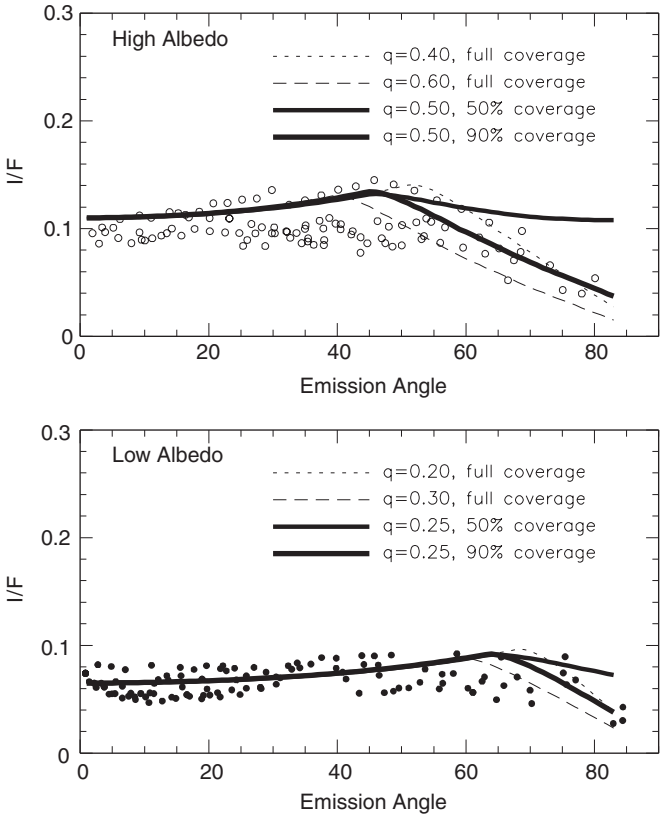

Fig. 7. Roughness scans extracted from Ta for bright and dark areas, shown with the roughness model for various values of q and surface fractional coverage.

angles to derive macroscopic roughness. On the contrary, disk-resolved measurements obtained by spacecraft are far more diagnostic of surface roughness than integral data sets, and they do not have the additional problem of non-uniqueness of fits because of other competing physical factors (e.g., the single particle phase function). For our first preliminary analysis of Titan's surface roughness, we consider roughness fits for the two major photometric terrains of Titan suggested by our albedo maps. The wavelength chosen was 2.01 μm, because the haze opacity is low and the signal-to-noise relatively high; of course macroscopic roughness should not depend on the wavelength chosen.

Fig. 7 shows a group of scans of specific intensity compared with data extracted for both high- and low-albedo regions, corrected for the effects of haze. I/F, emission angle, incidence angle, and solar phase angle were extracted for each point in the scans. The solar phase angle does not change by more than a degree, but the emission angle covers nearly a full range from 0° to 90°, while the incident angle covers a smaller range (10°–30°). The high-albedo data were extracted primarily from Xanadu, which appears on the lower right of the Ta mosaic in Fig. 2, while the low-albedo data were extracted mainly from Shrangra-La, the dark equatorial region. Each data point in the theoretical scan was computed for the appropriate geometry and is shown plotted as a function of emission angle. A value of $f(\alpha)$ of 0.23 and 0.32 were used to normalize the theoretical scans for the dark and bright regions, respectively. (The fairly small (~10%) haze correction is imperfect, as we have not considered effects such as emission from the haze, which is unknown without more detailed data and analyses. An analysis of the scans with no haze correction yields the same roughness parameters to within our errors, so our naïve haze subtraction does not affect the main results. The most important result—that the two albedo terrains have very different roughnesses—is a comparative one that is not sensitive to errors in the haze correction. As a complete radiative transfer model for Titan's atmosphere is developed, our results will be improved upon.) A best-fit roughness model was derived by generating families of curves corresponding to various depth-to-diameter (q) ratios, and fitting them by a least-squares method to the extracted curves. In addition to the depth-to-diameter ratio, the fraction of the surface covered by craters was altered. For the high-albedo region, $q = 0.5$, with nearly full (~90%) surface coverage provides a good average fit, with ranges in q from 0.4–0.55. The low-albedo region, $q = 0.25$, again with nearly complete surface coverage, provides the average best fit, with a range in q of 0.2–0.3.

Once the roughness has been determined for a specific region, it can be modeled and "subtracted" from the data set so that other parameters can be uniquely determined. For this study, I/F values and corresponding incidence, emission, and solar phase angles were extracted for bright and dark regions at a range of phase angles from the T0 observations to determine the surface phase function, $f(\alpha)$.

The surface phase function depends solely on the physical properties of the surface, namely macroscopic roughness, the compaction state of the particles in the optically active portion of the upper regolith, and the single particle phase function. The latter function is an indicator of particle properties, including their size, shape, and real and complex indices of refraction. At the moderately high solar-phase angles covered in the early Titan flybys, the sensitive parameters are macroscopic roughness and the single particle phase function (Helfenstein et al., 1988). The effects of surface particle compaction are exhibited at smaller solar-phase angles (especially $<10^{\circ}$, the region of the opposition surge) which will become observable later in the mission.

Again, the measurements at 2.01 μm were used because they represent the best combination of high signal-to-noise and low haze opacity. The upper left cell of Fig. 8 shows the phase function, computed by means of Eq. (1) and normalized by a factor that depends on the albedo of the surface. The upper right cell shows the phase curve corrected for haze. For comparison, the phase curves of Mimas, a typicalicy satellite, and the low albedo side of Iapetus are shown. (Again, our simple correction was used, but phase angles larger than 70° were eliminated because the forward-scattering phase function of the haze itself began to become apparent.) The lower left shows the phase function with the effects of roughness eliminated. To accomplish this correction, we computed the relative increase in intensity between a smooth surface ($q = 0$) and the average q of the low and high-albedo regions. This factor was applied to each data point, depending on whether it was in a high or low-albedo region. This determination was made from the geographical latitude and longitude of each point, which is computed by JPL's navigation software along with the incidence, emission, and solar phase angles. Locations inside Fensal Aztlan (the sideways "H" seen in the T5 mosaic) and the dark regions in the South Polar Region were designated as low-albedo. The remaining function is dependent solely on the single particle phase function:

$$f'(\alpha) = CP(\alpha), \tag{2}$$

where $P(\alpha)$ is the single particle phase function, and C is a constant that depends on the single-scattering albedo that will be derived when more data are collected from future flybys and a more complete radiative transfer model is in hand. The lower right cell of Fig. 8 shows the single-particle-phase function fit to a Henyey–Greenstein-phase

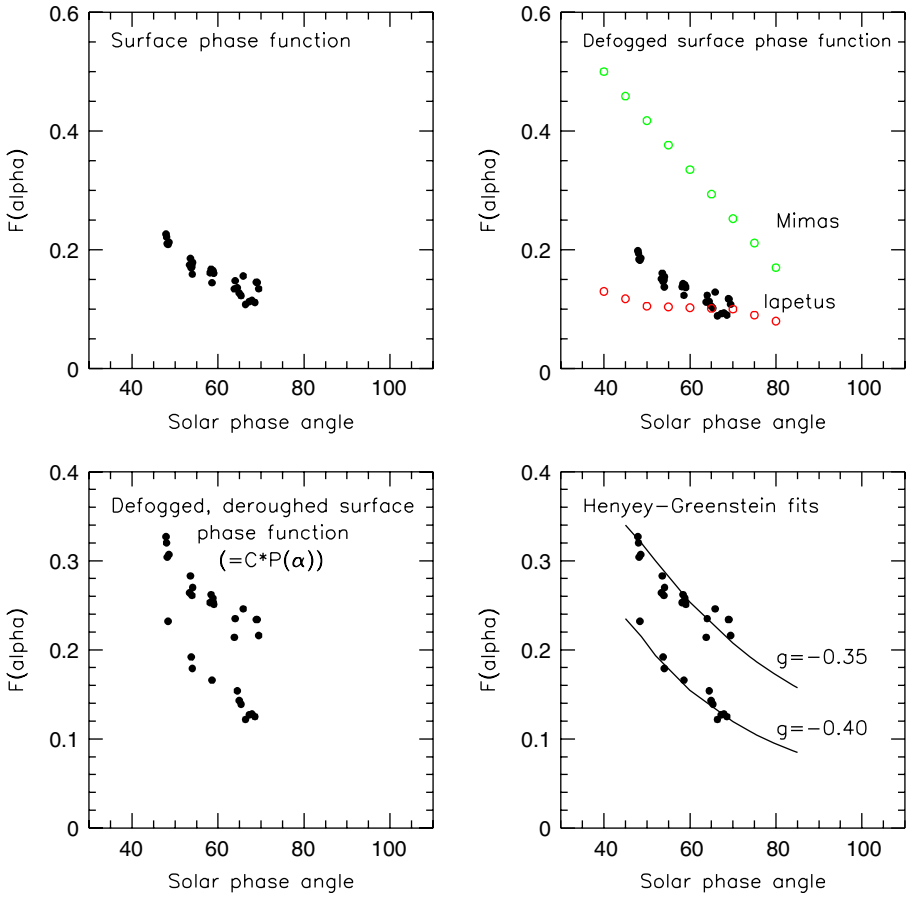

Fig. 8. $F(\alpha)$ for Titan's surface (upper left). The upper right cell shows the haze corrected values, while the lower left shows $f(\alpha)$ and with roughness eliminated. The lower right panel shows the corrected values with Henyey–Greenstein fits. The values for Mimas and Iapetus are from Buratti (1984) and Squyres et al. (1984), respectively.

function given by

$$P(\cos\theta, g) = (1-g^2)/(1+g^2-2g\cos\theta)^{3/2}, \quad (3)$$

where the scattering angle $\theta = (180^\circ - \alpha)$ and g is the asymmetry factor describing the directional scattering properties of individual particles. A g of -1 corresponds to pure backscattering, $+1$ corresponds to pure forward scattering, and 0 describes isotropic scattering. The backscattering properties of a surface depend on the nature of the particles comprising the optically active portion of the regolith; brighter surfaces and smaller particles tend to scatter more isotropically. Virtually, all planetary surfaces are predominately backscattering, although a notable exception is one region of comet 19P/Borrelly, which appears to be laden with small native dust particles that scatter nearly isotropically (Buratti et al., 2004).

The best-fit results show that the surface of Titan is, like other satellite surfaces, backscattering. The most significant result is that the single-particle-phase function of both high- and low-albedo regions is very similar, with a value of -0.35 ± 0.03 for the bright regions, and -0.40 ± 0.03 for the dark regions. The optically active portion of Titan's upper surface is thus globally similar, even though there is a marked difference in the roughness of the bright and dark regions of Titan. As an excursion in solar phase angles is obtained for specific regions on Titan's surface during the next $2\frac{1}{2}$ years of observations, these preliminary results can be expanded.

3.4. The composition of Titan's surface

Although a detailed analysis of the composition of Titan's surface is beyond the scope of this paper (instead, see McCord et al., 2006) the haze-corrected $f(\alpha)r_n$ function discussed above can be extracted from each atmospheric window and compared to various ices and other materials to seek consistent spectral fits. Fig. 9 shows this spectrum of Titan at several different solar-phase angles: one spectrum was obtained for bright regions, and three others were obtained for low-albedo regions (the haze corrections were accomplished with the haze opacities of Griffith et al., 2003, augmented by values of 25% per unit airmass for 2.73 and 2.9 μm). Although methane, ammonia, and carbon dioxide ice laboratory spectra do not match the spectrum of Titan extracted through the windows, water ice offers a moderately good fit, especially when Titan tholins (Cruikshank et al., 1991) are added to the spectral mix, in agreement with the results of Griffith et al. (2003). When water ice is combined with Titan tholins in a 2:1 ratio with a simple linear mixing model, the fit is reasonable (Fig. 9). (The water ice spectrum used in the model was obtained from the United States Geologic Survey's spectral library, and the model spectra were normalized to the brightest spectrum at 2 μm.) Methane clathrate or ammonia hydrate, which is difficult to distinguish from water ice, particularly for a spectrum observed only through the atmospheric windows, could also be present. We note that there are problems with our spectral model. For example, the shape of the spectrum at the 2.69–2.75 μm spectral window (see Fig. 1) does not match that of water ice + tholin; another as yet unidentified material must be present. (See McCord et al., 2006 for more details.)

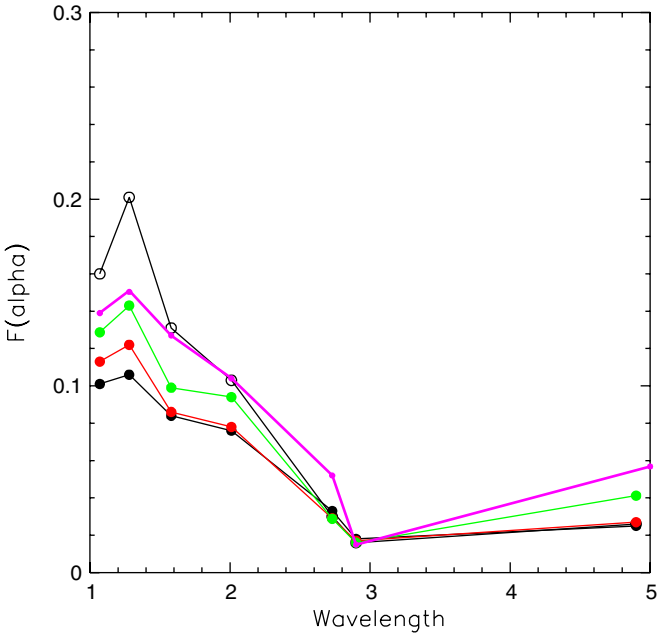

Fig. 9. The haze-corrected spectrum of Titan through the atmospheric windows. The spectra were extracted for one high albedo regions and three low albedo regions, and are given in units of $f(\alpha)r_n$. The linear mixing model (magenta) contains 66% water ice and 34% Titan tholin.

4. Discussion and conclusions

The first spacecraft observations of Titan in the near infrared region of the spectrum enable whole new fields of inquiry, including quantitative measurements of surface albedo, photometric modeling, compositional mapping, and geophysical analysis. In this paper we have analyzed data through the atmospheric windows to obtain preliminary results on the first two areas of inquiry.

The surface albedo of Titan is low in the infrared region of the spectrum, as is that of other icy saturnian satellites (Clark et al., 2005). At 2.01 μm we find an average normal reflectance of 0.15 ± 0.02, while at 2.73 μm the albedo is only 0.035. All wavelengths exhibit two distinct albedo regimes on the surface. The rotational lightcurve of Titan, which was known from ground-based observations, shows a hemispheric dichototomy that is due to a preponderance of high-albedo material on the leading side of Titan.

Photometric models of planetary surfaces have been widely used over the past two decades to derive physical properties, including macroscopic roughness and surface particle sizes and compaction states. The VIMS data enable the first of such studies for Titan. Using a roughness model first developed by Buratti and Veverka (1985), we have derived average macroscopic roughness for both

Table 2
Selected photometric roughness and particle phase functions for comparison

Object	$q = h/R$	Mean slope angle,$\theta(^\circ)$	g(-1 = backscattering, $+1$ = forwardscattering)	References
Titan (bright)	0.50 ± 0.10	34	-0.35 ± 0.03	This work
Titan (dark)	0.25 ± 0.05	18	-0.40 ± 0.03	This work
Moon (bright)		24	-0.33	Helfenstein and Veverka (1987): roughness; Hillier et al. (1999): g
Moon (dark)		8	-0.22	Helfenstein and Veverka (1987): roughness; Hillier et al. (1999): g
Europa	0.30	22	-0.43	Buratti (1985): roughness; Domingue et al. (1991): g
Mimas		30	-0.21	Verbiscer and Veverka (1992)

Previous results are in the visible region of the spectrum.

high- and low-albedo terrains. The two terrains are distinctly different: the bright terrain is very rough, with a mean depth to radius ratio (q) of 0.5, while the low-albedo terrain is relatively smooth, with a mean q of 0.25. (A simple mathematical calculation shows that these numbers are equivalent to a Hapke mean slope parameter (Hapke, 1984) of 34° and 18°, respectively.) Spatially resolved determinations of roughness for the Moon yield the only case that shows a difference this large. The lunar bright terrains (mainly highlands) yield an average slope angle of 24°, while the dark terrains (mainly maria, which are basaltic lava flows) exhibit a mean slope angle of 8° (Helfenstein and Veverka, 1987). As for the Moon, the results for Titan imply different geologic histories for the two terrains. The bright region may exhibit a large degree of roughness because it contains many deeply cut drainage features, while the low-albedo terrain exhibits a much flatter surface because it contains catch basins for debris flowing from the drainage networks. Perhaps the low-albedo region contains subsurface liquid that cause slumping of surface features, or it is the bottom of a basin that was once filled with liquid. Although our own results are preliminary and somewhat speculative, they are supported by stereo images from the Huygens Lander showing that the bright terrain has anomalously large slope angles and deep features (Soderblom, 2005). Table 2 summarizes some of the previous results on physical photometric parameters for satellites. These previous results are all in the visible region of the spectrum. Although roughness is not dependent on wavelength and can be directly compared, the phase functions may vary with wavelength and thus cannot be quantitatively compared.

The single particle phase function of Titan is backscattering, and it is similar to that of other icy satellites (derived in the visible region), as well as that of rocky bodies. Unlike the case for surface roughness, the particle-phase function appears to be fairly uniform over the surface of Titan (the low-albedo regions may be slightly more backscattering). This result implies that the surface is coated with particles, perhaps dust, or a film. There are several possible explanations for this coating: particles from Titan's haze layer could be raining down on its surface to create a layer or a film. Another possibility is eolian transport of particles, as on Mars, which is coated with a layer of dust that causes it to be spectrally similar. The Cassini Radar experiment has detected numerous "cat scratches" on Titan; they appear to be wind-blown dunes (Elachi et al., 2005).

The physical parameters derived in this paper are preliminary: a full radiative transfer model that more precisely corrects for the atmosphere and haze—and enables a quantitative analysis of spectral regions where the haze is more opaque—and the acquisition of additional data will enable a more precise and extensive analyses. In any case, the roughness and backscattering properties of Titan imply that its surface is entirely, or nearly entirely, solid at the present epoch, although our results are consistent with the placement of small channels or ponds of liquid on Titan's surface.

Acknowledgements

We thank Dr. Sylvain Douté for his detailed and thoughtful review of our paper, and Dr. Michel Combes for suggesting and leading a special issue on VIMS Titan results. Part of this work was carried out at the Jet Propulsion laboratory, California Institute of Technology, under contract to the National Aeronautics and Space Administration.

References

Brown, R.H., et al., 2004. The Cassini visual and infrared mapping spectrometer (VIMS) investigation. Space Sci. Rev. 115, 111–168.
Buratti, B.J., 1984. Voyager disk resolved photometry of the Saturnian satellites. Icarus 59, 426–435.
Buratti, B.J., 1985. Application of a radiative transfer model to bright icy satellites. Icarus 61, 208–217.
Buratti, B.J., Hicks, M.D., Soderblom, L.A., Britt, D., Oberst, J., Hillier, J.K., 2004. Deep space 1 photometry of the nucleus of Comet 19P/Borrelly. Icarus 167, 16–29.

Buratti, B.J., Veverka, J., 1985. Photometry of rough planetary surfaces: the role of multiple scattering. Icarus 64, 320–328.

Campbell, D.B., Black, G.J., Carter, L.M., Ostro, S.J., 2003. Radar evidence for liquid surfaces on Titan. Science 302, 431–434.

Clark, R.N., et al., 2005. Compositional mapping of surfaces in the Saturn system with Cassini VIMS: the role of water, cyanide compounds and carbon dioxide. American Geophysics, Union Fall Meeting, abstract #P22A-02.

Coustenis, A., Hirtzig, M., Gendron, E., Drossart, P., Lai, O., Combes, M., Negrão, 2005. Maps of Titan's surface from 1–2.5 μm. Icarus 177, 89–105.

Cruikshank, D.P., Allamandola, L.J., Hartmann, W.K., Tholen, D.J., Brown, R.H., Matthews, C.N., Bell, J.F., 1991. Solid C triple bond N bearing material on outer solar system bodies. Icarus 94, 345–353.

Domirgue, D.L., Hopke, B.W., Lockwood, G.W., Thompson, D.T., 1991. Europa's phase curve: Implications for surface structure. Icarus 90, 30–42.

Elachi, C., et al., 2005. Cassini Radar views the surface of Titan. Science 308, 970–974.

Gibbard, S., de Pater, I., Macintosh, B.A., Roe, H.G., Max, C.E., Young, E.F., McKay, C.P., 2004. Titan's 2 μm surface albedo and haze optical depth in 1996–2004. Geophys. Res. Lett. 31, L17S02.

Griffith, C.A., Owen, T., Geballe, T.R., Raynes, J., Rannou, P., 2003. Evidence for the exposure of water ice on Titan's surface. Science 300, 628–630.

Hapke, B., 1984. Bidirectional reflectance spectroscopy. 3. Correction for macroscopic roughness. Icarus 59, 41–59.

Helfenstein, P., Veverka, J., 1987. Photometric properties of lunar terrains derived from Hapke's equation. Icarus 72, 342–357.

Helfenstein, P., Veverka, J., Thomas, P., 1988. Uranus satellites: Hapke parameters from Voyager disk integrated photometry. Icarus 74, 231.

Hillier, J.K., Burath, B.J., Hill, K., 1999. Multispectral photometry of the Moon and absolute calibration to the Clementine UV/Vis Camera. Icarus 141, 205–225.

Lellouch, E., Schmitt, B., Coustenis, A., Cuby, J.-G., 2004. Titan's 5-micron lightcurve. Icarus 168, 209–214.

Lemmon, M.T., Karkosochka, E., Tomasko, M., 1993. Titan's rotation: surface feature observed. Icarus 103, 329–332.

Lemmon, M.T., Karkosochka, E., Tomasko, M., 1995. Titan's rotational light-curve. Icarus 113, 27–38.

McCord, T.M., et al., 2006. Composition of Titan's surface from Cassini VIMS. Planet. Space Sci., this issue.

Roe, H.G., de Pater, I., Gibbard, S.G., Macintosh, B.A., Max, C.E., Young, E.F., Brown, M.E., Bouchez, A.H., 2004. A new 1.6 μm map of Titan's surface. Geophys. Res. Lett. 31, L17S03.

Shepard, M.K., Campbell, B.A., 1998. Shadows on a planetary surface and implications for photometric roughness. Icarus 134, 279–291.

Simonelli, D.P., et al., 2004. The roughness of phoebe as determined by Cassini VIMS. B.A.A.S. 36, abstract # 4.03.

Smith, P.H., Lemmon, M.T., Lorenz, R.D., Sromovsky, L.A., Caldwell, J.J., Allison, M.D., 1996. Titan's surface revealed by HST imaging. Icarus 119, 336–346.

Soderblom, L., 2005. Titan's surface as viewed from the Huygens probe by the descent imager/spectral radiometer. Geological Society of America Annual Meeting, Talk 102–9. Salt Lake City, UT, October 17, 2005.

Squyres, S.W., Buratti, B.J., Veverka, J., Sagan, C., 1984. Voyager photometry of Iapetus. Icarus 61, 426–435.

Sotin, C., et al., 2005. Release of volatiles from a possible cryovolcano from near-infrared imaging of Titan. Nature 435, 786–789.

Verbiscer, A., Veverka, J., 1992. Mimas: photometric roughness and albedo map. Icarus 99, 63–69.

Veverka, J., Goguen, J., Young, S., Elliot, J., 1978. Scattering of light from particulate surfaces. I. A laboratory assessment of multiple-scattering effects. Icarus 34, 406–414.

West, R.A., Brown, M.E., Salinas, S.V., Bouchez, A.H., Roe, H.G., 2005. No oceans on Titan from the absence of a near-infrared specular reflection. Nature 436, 670–672.